HHS Public Access

Author manuscript

Sens Actuators Rep. Author manuscript; available in PMC 2025 April 15.

Published in final edited form as:

Sens Actuators Rep. 2024 December ; 8: . doi:10.1016/j.snr.2024.100212.

Rapid and portable quantification of HIV RNA via a smartphone-enabled digital CRISPR device and deep learning

Hoan T. Ngo[a], **Patarajarin Akarapipad**[b], **Pei-Wei Lee**[a], **Joon Soo Park**[b], **Fan-En Chen**[b], **Alexander Y. Trick**[a], **Tza-Huei Wang**[a,b,c,*], **Kuangwen Hsieh**[a]

[a]Department of Mechanical Engineering, Johns Hopkins University, Baltimore, MD 21218, USA

[b]Department of Biomedical Engineering, Johns Hopkins University, Baltimore, MD 21218, USA

[c]Institute for NanoBioTechnology, Johns Hopkins University, Baltimore, MD 21218, USA

Abstract

For the 29.8 million people in the world living with HIV/AIDS and receiving antiretroviral therapy, it is crucial to monitor their HIV viral loads. To this end, rapid and portable diagnostic tools that can quantify HIV RNA are critically needed. We report herein a rapid and quantitative digital CRISPR-assisted HIV RNA detection assay that has been implemented within a portable smartphone-based device as a potential solution. Specifically, we first developed a fluorescence-based reverse transcription recombinase polymerase amplification (RT-RPA)-CRISPR assay that can efficiently detect HIV RNA at 42 °C. We then implemented this assay within a commercial stamp-sized digital chip, where RNA molecules were quantified as strongly fluorescent digital reaction wells. The isothermal reaction condition and the strong fluorescence in the digital chip simplified the design of thermal and optical modules, allowing us to engineer a palm-size device measuring 70 × 115 × 80 mm and weighing less than 0.6 kg. We also capitalized the smartphone by developing a custom app to control the device, perform the digital assay, and capture fluorescence images throughout the assay using the smartphone's camera. Moreover, we trained and verified a deep learning-based algorithm for analyzing fluorescence images and identifying positive digital reaction wells with high accuracy. Using our smartphone-enabled digital CRISPR device, we successfully detected as low as 75 copies of HIV RNA in just 15 min,

*Corresponding author. thwang@jhu.edu (T.-H. Wang).

Declaration of generative AI and AI-assisted technologies in the writing process

During the preparation of this work the authors used ChatGPT (OpenAI) to improve readability and language. After using this tool/service, the authors reviewed and edited the content as needed and take full responsibility for the content of the publication.

CRediT authorship contribution statement

Hoan T. Ngo: Conceptualization, Methodology, Software, Investigation, Formal analysis, Writing – original draft, Writing – review & editing. **Patarajarin Akarapipad:** Methodology, Investigation, Formal analysis. **Pei-Wei Lee:** Methodology, Investigation, Formal analysis. **Joon Soo Park:** Resources, Methodology. **Fan-En Chen:** Resources, Methodology. **Alexander Y. Trick:** Resources, Methodology. **Tza-Huei Wang:** Writing – review & editing, Supervision, Funding acquisition. **Kuangwen Hsieh:** Conceptualization, Writing – original draft, Writing – review & editing, Visualization, Supervision, Funding acquisition.

Declaration of competing interest

The authors declare that they have no known competing financial interests or personal relationships that could have appeared to influence the work reported in this paper.

Supplementary materials

Supplementary material associated with this article can be found, in the online version, at doi:10.1016/j.snr.2024.100212.

showing its potential toward monitoring of HIV viral loads and aiding the global effort to combat the HIV/AIDS epidemic.

Keywords

Point-of-care diagnostics; HIV viral load monitoring; RT-RPA isothermal amplification; CRISPR-based diagnostics; Smartphone-based medical device; Deep learning

1. Introduction

With approximately 39.0 million people living with HIV/AIDS across the globe, HIV/AIDS remains one of the leading global public health threats [1]. Fortunately, revolutionary advances in HIV antiretroviral therapy (ART) in the past two decades have turned this once deadly disease into a manageable chronic condition [2]. Nevertheless, for the 29.8 million people living with HIV/AIDS who are receiving ART in the world [1], access to HIV viral load quantification is essential to monitoring ART efficacy, detecting viral rebound, and preventing onward transmission. As a result, the World Health Organization has stressed the critical need for diagnostic tools that can enhance the accessibility to HIV viral load quantification for individuals living with HIV/AIDS [3].

Diagnostic tools designed to improve the accessibility to HIV viral load monitoring should be rapid, quantitative, and portable. Existing commercial platforms such as GeneXpert or m-PIMA that use RT-PCR to detect HIV are mainly confined to laboratory settings with limited portability and accessibility. In the research arena, current portable platforms [4–11] utilizing either RT-PCR or RT-LAMP (loop mediated isothermal amplification) generally employ bulk-based reactions, which lack accurate quantification and can be slow when detecting targets of low concentrations. These drawbacks call for alternative solutions for HIV viral load monitoring.

Compared to bulk-based reactions, digital reactions have the advantage of analyzing individual copies of targets, allowing for more accurate quantification. Indeed, digital PCR and digital LAMP have been employed for quantitative detection of various pathogens [12–17], including HIV [18,19]. Among digital reactions, digital CRISPR assays have in recent years emerged as a novel option and have demonstrated quantitative detection with wide dynamic range and rapid assay time [20–24]. Despite these advantages, digital CRISPR assays to date have predominantly relied on bulky instrumentation, such as fluorescence microscopy. While smartphones have been utilized to develop portable digital PCR and digital LAMP devices [14,25–27], the development of smartphone-enabled digital CRISPR devices is in its infancy, with no reported use for HIV viral load quantification, and the speed of the assay has yet to be explored.

In this study, we present a smartphone-enabled digital CRISPR device for rapid and portable quantification of HIV RNA (Fig. 1). Our platform employs a fluorescence-based reverse transcription recombinase polymerase amplification (RT-RPA)-CRISPR HIV assay for the detection of HIV RNA. We systematically optimized the assay conditions to enhance the speed of HIV RNA detection. Subsequently, we implemented this accelerated assay in a

commercially-available, stamp-sized microfluidic digital chip specifically repurposed for this study. To perform a portable, digital CRISPR assay, we developed compact, palm-sized instrument comprising a heating module, a fluorescence imaging module, a rechargeable battery, and a smartphone. Additionally, we developed a custom smartphone application for convenient device control and implemented a deep learning (DL)-based algorithm to accurately quantify HIV RNA within the digital chip. Using our smartphone-enabled digital CRISPR device, we achieved detection of HIV RNA at levels as low as 75 copies within 15 min.

2. Results and discussion

2.1. Overview of workflow

HIV viral load can be quantified via our smartphone-enabled digital CRISPR device through a simple workflow (Video S1). First, HIV RNA and RT-RPA-CRISPR assay reagents – including RT-RPA reagents, CRISPR/Cas12a effector and guide RNAs, and single-stranded DNA (ssDNA) fluorogenic reporter – are loaded into a digital chip, where individual RNA molecules are digitized into digital reaction wells in accordance with Poisson distribution (Fig. 1A). Next, the digital chip is inserted into the smartphone-based device. Key parameters such as the reaction temperature, fluorescence imaging frequency, and the reaction time can be configured through a custom smartphone app installed on the smartphone (Fig. 1B). Upon initiating the assay, the device automatically regulates the set reaction temperature for digital RT-RPA-CRISPR (e.g., 42 °C) and captures fluorescence images at the set frequency (e.g., every 1 min) throughout the set reaction time (e.g., 15 – 60 min). Through digital RT-RPA-CRISPR, HIV RNA molecules are reverse transcribed and amplified, which activate Cas12a to cleave the fluorogenic reporter, thus yielding strong fluorescence within digital reaction wells (i.e., positive wells). At the conclusion of the assay, fluorescence images are analyzed using DL to count positive wells within the digital chip, which correspond to the amount of HIV RNA and hence the viral load (Fig. 1C).

2.2. Rapid RT-RPA-CRISPR HIV RNA detection assay

We first developed a fluorescence-based RT-RPA-CRISPR assay that can efficiently detect HIV RNA in a single-step within one pot. In this work, we targeted the HIV-1 *gag* gene (Fig. 2A) and employed previously reported RPA primers [28,29] and CRISPR/Cas12a guide RNAs [28] for detecting this target gene (Fig. 2B and Table S1). Using these primers and guide RNAs, we performed real-time RT-RPA-CRISPR on benchtop to observe the reaction kinetics from detecting 1000 copies HIV RNA – a comparable concentration to that of a single RNA copy within the digital reaction well. Based on this approach, we modified the reverse transcriptase, reaction temperature, reverse transcriptase concentration, and fluorogenic reporter of the assay in a step-by-step manner to improve the assay speed. Upon assay tuning, we used WarmStart RTx reverse transcriptase [30] at 0.75 U/μL in our RT-RPA-CRISPR and incubated it at 42°C (Figs. 2C – 2E and Figures S1 – S3). Additionally, based on prior screening of ssDNA fluorogenic reporters [31], we adopted the ssDNA fluorogenic reporter with the strongest fluorescence signal (i.e., TCCCT) in our RT-RPA-CRISPR and empirically found that it led to faster RT-RPA-CRISPR than a widely used ssDNA fluorogenic reporter (i.e., TTATT), likely because activated Cas12a

could cleave this reporter at a higher rate (Fig. 2F and Figure S4). Using our tuned RT-RPA-CRISPR, we could rapidly detect 1000 copies HIV RNA, where onset of fluorescence signal could be observed in ~10 min and plateau of fluorescence signal could be observed in ~30 min.

2.3. Palm-size smartphone-enabled digital device

We next developed a palm-size yet fully integrated device toward realizing digital RT-RPA-CRISPR. To do so, we first selected the smartphone and the digital chip for our device. For the smartphone, we selected Samsung Galaxy S10 for this work, as this smartphone features a 12-megapixel camera and offers flexible manual adjustments during photo acquisition. For the digital chip, we opted for commercially available QuantStudio digital chips that are equipped with 750-pL reaction wells arranged in an array of 20,000 wells, as commercial digital chips offer convenience and accessibility when compared to custom microfluidic digital chips. Based on the smartphone and the digital chip, we then designed the integrated device – composed of a macro lens, a LED, a LED driver, a custom miniature filter cube, a heater, a control circuitry featuring a TinyPICO microcontroller, and a rechargeable battery pack (Fig. 3A) – and packaged the device within a 3D-printed housing. This portable device measures 70 mm × 115 mm × 80 mm ($W \times L \times H$) and weighs 575 gs including the smartphone.

With the aid of the macro lens, the LED, and the custom miniature filter cube, the smartphone becomes capable of imaging the entire digital chip. Toward developing this fluorescence imaging capability, we note that an inexpensive, consumer-grade macro lens that is typically used for recreational macrophotography provided both sufficient field of view and satisfactory resolution, thus allowing us to obviate more complex lenses in our device. We identified the appropriate macro lens by evaluating four consumer-grade macro lenses that are compatible with our smartphone. For evaluation, we used these macro lenses at brightfield to capture images of a standard resolution target and a standard distortion target at their maximum and minimum working distances (Figure S5). Subsequent image analysis allowed us to compare their resolution, distortion, field of view, and range of working distance (Figure S6). After evaluation, we selected a macro lens that, in combination with the camera lens, achieved a resolution of 36.0 line pairs/mm (corresponding to a line width of 13.9 μm), exhibited 0.99 % pincushion distortion, and provided a field of view measuring 22 mm by 16.5 mm at a working distance of 19 mm (Figures S7 and S8). The resolution and the field of view are sufficient for the 60 μm-wide digital reaction wells and the 10 × 10 mm array area of the QuantStudio digital chip, while the working distance is sufficient for accommodating the custom miniature filter cube, which measure 17.5 mm in height. We subsequently assembled the macro lens, the LED, and the custom miniature filter cube into a full “fluorescence macrophotography module” and verified its performance by detecting a QuantStudio digital chip loaded with 10 μM Cy5 fluorescence dye, a concentration comparable to the reporter concentration in our RT-RPA-CRISPR. We were indeed able to capture the image of the entire chip while resolving individual digital reaction wells (Figs. 3B and 3C), as indicated by the stronger fluorescence signals in digital reaction wells (gray value = 71.40 ± 1.62, $n = 12$) than the

pitches between the adjacent digital reaction wells (gray value = 52.88 ±3.64, $n = 13$; Fig. 3C).

In our device, we employed a positive temperature coefficient (PTC) ceramic heater [32–35] for heating digital RT-RPA-CRISPR. For our PTC ceramic heater, we characterized its temperature uniformity across the heater region, its warm-up time, and its temperature variability as a function of time. The PTC ceramic heater region – located at the center of its aluminum casing (Figure S9) – delivered sufficiently uniform temperature (Fig. 3D, spatial coefficient of variation = 11.4 %). During the course of a 60 min incubation, the PTC ceramic heater reached the set temperature (set at 43 °C during initial characterization) in ~3 min and maintained the temperature at 43.04 ± 0.13 °C thereafter (Fig. 3E, temporal coefficient of variation = 0.31 %).

Finally, we assembled a simple control circuitry and developed a custom smartphone app to control all components within the device (Fig. 3F). Here, the control circuitry features a TinyPICO ESP32 microcontroller that is powered by the rechargeable battery pack to regulate the temperature of the PTC ceramic heater, switch the LED on and off, and communicate with the smartphone via Bluetooth (see Figure S10 for the program flowchart of the TinyPICO microcontroller). The smartphone app, which was written in the MIT App Inventor 2 environment, enables users to configure assay parameters including temperature, time, and fluorescence imaging frequency. Once the user sets these parameters and initiates the assay, the app transmits the parameters to the TinyPICO microcontroller, which uses a PID (proportional-integral-derivative) controller to control the temperature of the PTC ceramic heater. Once the set temperature is reached, the TinyPICO microcontroller activates the LED for fluorescence excitation and simultaneously notifies the app to activate the camera and capture fluorescence images according to the specified imaging frequency (Figure S11). Throughout the duration of the assay, the app also updates the system status and displays the most recent fluorescence image (Figure S12).

2.4. Facile identification of positive digital wells

We next demonstrated the capability of our assembled smartphone-enabled digital device (Fig. 3G) in performing digital RT-RPA-CRISPR in QuantStudio chips and detecting HIV RNA. To this end, we first focused on the fluorescence detection capability of the fluorescence macrophotography module in the smartphone-enabled digital device by incubating digital RT-RPA-CRISPR in QuantStudio chips on a commercial flatbed thermocycler and then qualitatively comparing end-point fluorescence imaging results with a fluorescence microscope. We observed comparable detection of strongly fluorescent positive wells corresponding to the presence of HIV RNA between the fluorescence macrophotography module and the fluorescence microscope (Figure S12), which supports the fluorescence detection capability of our device. We then used our device to directly incubate and image digital RT-RPA-CRISPR in QuantStudio chips. At the conclusion of 60-min digital RT-RPA-CRISPR, we observed positive wells with strong fluorescence (~2.5 times higher than the background), signifying positive results and confirming the successful amplification and detection of HIV RNA (Fig. 4A). We additionally tested different HIV RNA concentrations and confirmed via fluorescence microscopy. The results

further demonstrate successful digital RT-RPA-CRISPR conducted in our device, while also suggesting that our device performed comparably to benchtop instruments (Figure S13).

With the advent of DL, we explored the feasibility of DL-facilitated analysis of our smartphone-acquired fluorescence images and detection of positive wells. In this work, we chose YOLOv5 objection detection model as our DL algorithm. YOLO [36] is a series of models that achieve object detection using a single neural network that predicts bounding boxes coordinates and class probabilities directly from images in one evaluation. Thus, YOLO models are faster and more lightweight than most other object detectors [37]. Moreover, YOLOv5 has recently been employed to detect microfluidic droplets [38,39] – similar objects as our digital reaction wells. Thus, we hypothesize that YOLOv5 can be trained to classify strongly fluorescent positive reaction wells as the objects from each fluorescence image and then output the number of detected positive wells from each image. To train our YOLOv5 object detection model, given the small sizes of the positive wells in the full images, we employed an image tiling technique [40] that has been demonstrated to facilitate accurate detection of small objects in images (Figure S14). In parallel, we manually counted positive wells as the true class in this work (Figure S15). Upon training, our DL algorithm correctly identified the majority of the manually counted positive wells (i.e., true positive, TP; Fig. 4B). It was also capable of accurately identifying positive wells that were in close proximity. Nevertheless, our algorithm still misidentified several false positive (FP) wells and false negative (FN) wells (Fig. 4B). For quantitative assessment of our DL algorithm, we first chose accuracy – the ratio between the correct results and the total results – as a natural evaluation metric. Additionally, we recognized that because we focused on detecting only the positive wells, our data that lacked true negative (TN) wells were imbalanced and thus could be evaluated via F1 score as an alternative to accuracy [41,42]. For our initial result, our DL algorithm achieved accuracy of 0.908 and F1 score of 0.952 (Fig. 4C). Subsequently, we performed a total of 4 technical replicates using 7500 copies of HIV RNA and assessed our DL algorithm. Across these 4 replicates, our DL algorithm achieved accuracies of at least 0.897 and F1 scores of at least 0.946 (Fig. 4D and Figure S16). Moreover, we performed replicates using 750 copies of HIV RNA and our DL algorithm achieved comparable accuracies and F1 scores (Figure S17). These results provide solid support for the feasibility of DL-facilitated analysis of our smartphone-acquired fluorescence images and detection of positive wells.

We note that, in addition to DL, we could also employ a standard ImageJ- and thresholding-based method for analyzing our smartphone-acquired fluorescence images (Figure S18). Here, we utilized auto thresholding and particle analysis functions in ImageJ to detect the positive wells. Upon selecting an adequate threshold, our thresholding-based method achieved adequate detection of positive wells (Figure S19). Nonetheless, our method with the selected threshold encountered minor difficulty in distinguishing positive wells that were close to each other. These results suggest that ImageJ- and thresholding-based method could be used to analyze our smartphone-acquired fluorescence images and detect positive wells, though more advanced threshold functions (e.g., auto local threshold and adaptive threshold) should be explored to further improve the detection performance.

2.5. Rapid and quantitative detection of HIV RNA

In addition to endpoint detection, our device could support real-time monitoring of digital RT-RPA-CRISPR and could provide a means to accelerate the assay time (Fig. 5A and Video S2). For demonstration, we performed digital RT-RPA-CRISPR for a sample containing 500 HIV RNA copies/μL, which is equivalent to 7500 copies of input HIV RNA per 15-μL reaction in the QuantStudio chip, and acquired fluorescence image in 1 min increment. We observed that the number of positive wells increased as a function of the reaction time until ~30 min and began to plateau after ~30 min (Fig. 5A). We subsequently quantified the percentage of positive wells at various time points normalized to the number of positive wells detected at 60 min for different input HIV RNA copy numbers. We found that ~39 % of positive wells were detectable by 10 min, ~71 % of positive wells were detectable by 15 min, and ~93 % of positive wells could be detected by 30 min (Fig. 5B). These results suggest that it is possible to achieve qualitative detection in as short as 10 min, though it would be preferable to employ 15 min assay time as this assay time could detect more positive wells and thus retain a better capacity for quantitative detection.

As the final demonstration, we performed quantitative detection HIV RNA in 15 min using our device. In these experiments, we tested 500, 250, 50, 5, 1, and 0 HIV RNA copies/μL, equivalent to 7500, 3750, 750, 75, 15, and 0 copies of input HIV RNA per 15-μL reaction in each QuantStudio chip. As expected, as the input RNA decreased, we observed fewer positive wells (Fig. 5C). Upon replicating the tests, we performed linear regression analysis and confirmed a linear relationship between the input RNA and the number of positive wells across the tested input HIV RNA concentrations (Fig. 5D). The results indicate that the dynamic range of our digital RT-RPA-CRISPR spans at least 2 orders of magnitude. Moreover, considering the QuantStudio chip houses 20,000 digital wells, the dynamic range can theoretically increase by at least another order of magnitude. We also determined the limit of detection as 75 copies of HIV RNA based on both calculating the conventional mean + 3SD threshold (Fig. 5D) and performing Student's *t*-tests (Figure S20). Indeed, the average number of positive wells measured from 75 copies of RNA lies above the threshold calculated from the no RNA negative controls. Meanwhile, we found that 75 copies of input HIV RNA were significantly different from the negative controls ($p < 0.01$). On the other hand, 15 copies of input HIV RNA failed to achieve sufficient significance when compared to the negative controls ($p > 0.05$). Finally, we performed benchtop RT-RPA-CRISPR and compared its performance. We found that although it was possible for benchtop RT-RPA-CRISPR to detect 5 copies/μL HIV RNA at 15 min, the fluorescence signals from 50 copies/μL and 250 copies/μL samples saw significant variations, which rendered the detection of these samples unreliable. Lengthening the reaction time to 60 min ensured that all samples could be detected, but the plateaued fluorescence signals inadvertently narrowed the dynamic range (Figure S21). Taken together, these results illustrate the advantages in speed and quantitation of digital RT-RPA-CRISPR in our device.

3. Conclusions

We report herein a smartphone-enabled digital CRISPR device for rapid and portable quantification of HIV RNA. Digitization of the CRISPR assay facilitated quantification

and accelerated the test speed, especially for low RNA concentrations. This improvement was achieved because each RNA molecule's digitization within a digital well generated a consistently high local concentration across the digital chip, making the assay speed independent of RNA concentration. Moreover, strong fluorescence signals generated from positive digital wells obviated fluorescence microscopy and allowed for a more portable means for detection. To this end, we developed the fluorescence macrophotography module to provide a simple and compact means for achieving both high resolution and a large field of view, enabling our smartphone to capture images of the entire QuantStudio digital chip while maintaining single-well resolution. As a result, our device demonstrated quantitative detection of HIV RNA in 15 min and a palm-sized footprint.

To our knowledge, this work represents the first smartphone-enabled digital CRISPR device for rapid and portable quantification of HIV RNA. Thus, while we note the advances, we also acknowledge several areas in need of future improvements. First and foremost, refinement of the current assay, chip, and device – such as enhancing assay efficiency such that all input RNA can be detected, obviating instrument-based chip loading, and improving signal-to-noise ratio by reducing the background light from the device material – remains an important objective. Second, incorporation of a streamlined sample preparation and enrichment process, such as HIV RNA extraction and concentration from blood, is crucial for future adoption for point-of-care use in clinical settings. Such a process could also improve detection sensitivity. To address this, a custom digital chip with integrated nucleic acid extraction capability [43] could be a viable solution. Third, enabling real-time HIV viral load reporting directly on the smartphone would enhance user-friendliness, as our current device requires completing a digital CRISPR reaction before analyzing fluorescence images. To this end, implementation of a deep learning (or machine learning) algorithm that is compatible with smartphones [44,45] and development of the algorithm such that it can directly detect of positive wells from fluorescence images represent a key objective. Fourth, acceleration of assay time could further enhance the usefulness of our method. To this end, further optimization of the assay speed and reduction of the time required to reach the set temperature represent viable strategies. Lastly, further reduction of the cost of our device would make it more affordable and thus accessible. Specifically, the material cost of our device is currently ~$700 USD without the smartphone (Table S2). This cost compares favorably to those of existing commercial platforms for deployment in clinical settings such as local health clinics. However, this cost is still too high for an accessible and point-of-care testing device. Cost reduction can be achieved by replacing expensive optical components with more cost-effective counterparts [46]. These improvements can strengthen the potential of our smartphone-enabled digital CRISPR device as a tool for the 29.8 million people in the world living with HIV/AIDS to monitor their HIV viral loads, thus contributing to the fight against HIV/AIDS.

4. Methods

4.1. Benchtop CRISPR-Cas12a-assisted RT-RPA assay

All oligonucleotides, including RPA primers, Cas12a-guide RNAs, and Alexa647-labeled single-stranded DNA (ssDNA) fluorogenic reporter, were purchased from Integrated DNA

Technologies (IDT; Coralville, IA). Both Cas12a-guide RNAs were modified with IDT's proprietary 5′ AltR1 and 3′ AltR2 modifications. Lyophilized Cas12a-guide RNA was reconstituted in DEPC-treated water (Thermo Fisher Scientific, Waltham, MA) at a concentration of 20 μM. Lyophilized DNA primers, DNA reporter, and DNA probe were reconstituted in nuclease-free water (Promega, Madison, WI) at a concentration of 100 μM. EnGen Lba (Lachnospiraceae bacterium ND2006) Cas12a (Cpf1) (M0653; 100 μM), WarmStart® RTx reverse transcriptase (M0380; 15,000 U/ml), Avian Myeloblastosis Virus (AMV) reverse transcriptase (M0277; 10,000 U/mL), and bovine serum albumin (BSA; B9000; 20 mg/mL) were purchased from New England BioLabs (Ipswich, MA). TwistAmp Basic kits were purchased from TwistDx Limited (Maidenhead, United Kingdom). All reconstituted oligonucleotides and the aforementioned reagents were stored at −20 °C.

To prepare a 10-μL reaction mixture for CRISPR-Cas12a-assisted RT-RPA, we utilized 1 × rehydrated TwistAmp Basic Reaction mix, 0.32 μM of each RPA primer, 0.64 μM of each Cas12a-guide RNA, 4 μM of Alexa647-labeled ssDNA fluorogenic reporter, 0.64 μM of EnGen Lba Cas12a, 0.75 U/μL of WarmStart RTx reverse transcriptase, 0.01 mg/mL of BSA, and 14 mM of MgOAc, unless otherwise specified (e.g., in Fig. S1 through S4). The assembly was conducted within a PCR hood (AirClean Systems, Creedmoor, NC). Initially, each dried pellet of TwistAmp Basic Reaction mix was reconstituted in 29.5 μL of rehydration buffer to prepare a 1.7 × rehydrated TwistAmp Basic Reaction mix. Subsequently, a master mix of all components except WarmStart RTx reverse transcriptase, BSA, and MgOAc was prepared in a 1.5 mL protein low-binding microcentrifuge tube (MilliporeSigma, Burlington, MA) and incubated at room temperature for 10 min to allow for the formation of Cas12a-guide RNA complexes. Following this, WarmStart RTx reverse transcriptase and BSA were added to the master mix. The master mix was transferred to a biosafety cabinet (The baker Company, Sanford, ME) to prevent contamination. Inside the biosafety cabinet, the master mix was divided into 8-μL MgOAc-free reaction mixture aliquots and supplemented with 1 μL of 140 mM MgOAc and 1 μL of 1000 copies/μL of synthetic HIV RNA (VR-3245SD, ATCC) to obtain the final 10-μL CRISPR-Cas12a-assisted RT-RPA reaction mixture.

4.2. Brightfield characterization of macro lens

To assess the resolution of the lenses, we utilized the USAF 1951 Glass Slide Resolution Targets from Edmund Optics (AZ). Each lens was attached to the smartphone camera and positioned approximately 3 cm away from the target to capture an image. The captured image was then analyzed using ImageJ software. A line was drawn across each set of the 3-line-pairs, and the line profile plot was generated using the "Analyze" option in ImageJ. To determine if the line pairs could be resolved, we calculated the mean and standard deviation of the maximum peaks (represented by white lines). Based on the empirical rule, assuming a normal distribution, the range of Mean ± 3 × Standard Deviation covers 99.7 % of the data. Therefore, if the minimum peaks (represented by black lines) fall within the 99.7 % range of the white lines, it indicates that they couldn't be completely distinguished from the white lines. In such cases, the resolution of the lens wo'ld be based on the line pair set prior to the one being evaluated.

The distortion percentage of the lenses was assessed using a Distortion Target from Edmund Optics (AZ). The evaluation involved calculating the distance from the center to the corner of the distortion target image, referred to as the image actual corner (AC), indicated by the blue arrow in Fig. S8. Additionally, the distance from the center to the edge corner (EC) was determined, indicated by the red arrow in Fig. S8. The distortion (D) is:

$$D(\%) = \frac{AC - EC}{EC} \times 100\% \quad (1)$$

4.3. Construction of the smartphone-based platform

Temperature measurement was performed using a thermistor (GA100K6MCD1, TE Connectivity) that was epoxied to a PTC heater (50 W AC DC 12 V, Bolsen Tech; purchased from Amazon; URL: https://tinyurl.com/yc797puw). A red LED (627 nm Rebel LED on a SinkPAD-II 20 mm Star Base – 53 lm @ 350 mA) was used for fluorescence excitation and was controlled by a 350 mA LED driver (BuckPuck 3021-d-E-350, LEDdynamics Inc.). The power supplied to the PTC heater and the LED driver was regulated by two N–CH MOSFETs (IRLB8721PBF, Infineon), which were controlled by a TinyPICO ESP-32 microcontroller (TinyPICO, Unexpected Maker). A macro lens (25X, MACTREM) was employed to focus the smartphone camera on the QuantStudio chip. The filter cube consisted of an excitation bandpass filter with a center wavelength of 624 nm and a 40 nm bandwidth, a dichroic filter at 660 nm, and an emission bandpass filter with a center wavelength of 692 nm and a 40 nm bandwidth (Edmund Optics). The entire platform was powered by a 12 V rechargeable Lithium-ion battery with a capacity of 3000 mAh (TalentCell).

Users were able to set the temperature, imaging frequency, and total analysis time using an app developed with MIT App Inventor 2 on a Samsung Galaxy S10 phone. These parameters were sent via Bluetooth to the TinyPICO ESP-32 microcontroller, which controlled the temperature of the PTC heater, activated the LED for fluorescence excitation, and instructed the smartphone to capture fluorescence images in real-time. In such real-time image acquisition experiments, the Taifun Camera extension was utilized to enable the app to access the smartphone camera. The smartphone camera was set to continuous-picture focus mode, auto white balance, and minimal exposure compensation for optimal performance. Source code of the smartphone app and the TinyPICO ESP-32 microcontroller program are provided in this link.

Alternatively, for end-point, single-image acquisition, the Pro mode of the built-in camera app on the Samsung Galaxy S10 phone was employed to achieve the best focus images. To do so, the smartphone camera focus was calibrated before conducting experiments. This calibration involved using a QuantStudio chip loaded with Cy5 fluorescence dyes. The chip was inserted into the platform, and with the LED turned on, the user captured images of the chip using the Pro mode of the built-in Camera app on the Samsung Galaxy S10 phone (ISO 400, 1/15 F1.5, white balance: A 4500 K). Manual focus adjustment was performed until

the image appeared the sharpest. After completing the smartphone camera focus calibration step, the platform was ready for use.

4.4. Detection of HIV RNA using the smartphone-based platform

To test the platform, a master mix was prepared, consisting of RPA buffer (1X), HIV forward and reverse primers (each at 0.32 μM), LbCas12a (0.64 μM), HIV crRNA1 and crRNA2 (each at 0.64 μM), Alexa647-labeled fluorogenic reporter (4 μM), WarmStart RTx reverse transcriptase (0.75 U/μL), BSA (0.01 mg/mL), Tween-20 (0.1 %), and DEPC-treated water. Subsequently, aliquots of the master mix (each 13.5 μL) were spiked with 0.75 μL of synthetic HIV RNA sequences containing 0, 15, 75, 750, or 7500 copies, along with 0.75 μL of 280 mM MgOAc. The samples were then loaded into QuantStudio 3D Digital PCR 20 K Chip v2 using the QuantStudio™ 3D Digital PCR Chip Loader following the user guide. The loaded QuantStudio chips were inserted into the platform for RT-RPA amplification at 42 °C for 60 min, with fluorescence imaging performed every 1 min.

4.4. Image analysis using deep learning

First, we trained a deep learning model based on YOLOv5 (Ultralytics) for object detection to detect positive wells in fluorescence images of the QuantStudio chip. Since the positive well objects in the QuantStudio chip fluorescence images are relatively small, we employed an image tiling approach during the training and deployment of the deep learning model (Figure S12). Specifically, we divided several fluorescence images (4032 pixels × 3024 pixels) into patches of size 416 pixels × 416 pixels, resulting in 143 tile images of 416 pixels × 416 pixels. Of note, this 416 pixels × 416 pixels patch size was selected because the positive wells were large relative to the patch and there were typically several positive wells in a patch, both of which facilitated effective detection of these positive wells by YOLOv5. The positive wells in these 143 tile images were labeled using a labeling tool. After labeling, the 143 tile images were divided into a training set (97 tile images), a validation set (26 tile images), and a testing set (20 tile images). Data augmentation techniques such as flipping, 90-degree rotation, cropping, adjusting brightness, exposure, blur, etc., were applied to the training set (with a maximum version size of 3×), resulting in a final set of 97 × 3 = 291 tile images for training. No data augmentation was applied to the validation and testing sets. The training was performed using Google Colab with 150 epochs (completed in 0.127 h), resulting in a mean Average Precision (mAP50) of 0.991 and mAP50–95 of 0.546.
For deployment, the weights of the trained model were exported and saved to a personal computer. A Python code was developed for (1) loading the fluorescence image of interest (4032 pixels × 3024 pixels), (2) dividing the image into 416 pixel x 416 pixel patches, (3) sequentially loading the image patches into the trained AI model for detecting positive wells in each image patch, (4) stitching the analyzed patches to create a 4032 pixel × 3024 pixel image with bounding boxes surrounding the predicted positive wells. To remove positive well predictions that are outside the chip region, we developed a Python code to estimate the chip region using auto thresholding followed by closing and erosion. Any positive well predictions that are outside the chip regions will be removed from the final output image. The analysis time was less than 1 min per 4032 pixel × 3024 pixel image. Source codes for training and deploying the deep learning model are provided in this link.

The deep learning model was evaluated by comparing each output image (i.e., predicted class) with its corresponding actual image (i.e., true class). Specifically, for each actual image, positive wells were manually counted using the cell counter tool in ImageJ. Then, the positive wells identified by the deep learning model were manually compared with the positive wells that were manually counted, from which true positive (TP) wells, false positive (FP) wells, and false negative (FN) wells. Of note, in this work, we focused on detecting only positive wells, so we considered true negative (TN) wells as 0. For evaluating the performance of the deep learning model, its accuracy and F1 score were computed based on the following equations:

$$Accuracy = \frac{TP + TN}{TP + FP + TN + FN} \tag{2}$$

$$F1Score = \frac{2 \times TP}{2 \times TP + FP + FN} \tag{3}$$

Supplementary Material

Refer to Web version on PubMed Central for supplementary material.

Acknowledgments

This work was supported by funding through the National Institutes of Health (R01AI138978, R01AI137272, and R61AI154628). K.H. is grateful for a developmental grant from the Johns Hopkins University Center for AIDS Research, a National Institutes of Health funded program (P30AI094189).

Data availability

Data will be made available on request.

References

[1]. UNAIDS, Global HIV & AIDS statistics — Fact sheet | UNAIDS. https://www.unaids.org/en/resources/fact-sheet. (Accessed September 18, 2023).

[2]. Deeks SG, Lewin SR, Havlir DV, The end of AIDS: HIV infection as a chronic disease, The Lancet 382 (2013) 1525–1533, 10.1016/S0140-6736(13)61809-7.

[3]. World Health Organization, Consolidated guidelines on the use of antiretroviral drugs for treating and preventing hiv infection: recommendations for a public health approach, 2nd ed, 2016. Geneva, Switzerland.

[4]. Drain Paul K, Dorward J, Bender A, Lillis L, Marinucci F, Sacks J, et al. , Point-of-Care HIV viral load testing: an essential tool for a sustainable global HIV/AIDS Response, Clin. Microbiol. Rev. 32 (2019), 10.1128/cmr.00097-18.

[5]. Hull IT, Kline EC, Gulati GK, Kotnik JH, Panpradist N, Shah KG, et al. , Isothermal amplification with a target-mimicking internal control and quantitative lateral flow readout for rapid HIV viral load testing in low-resource settings, Anal. Chem 94 (2022) 1011–1021. 10.1021/acs.analchem.1c03960. [PubMed: 34920665]

[6]. Kadimisetty K, Yin K, Roche AM, Yi Y, Bushman FD, Collman RG, et al. , An integrated self-powered 3D printed sample concentrator for highly sensitive molecular detection of HIV in whole blood at the point of care, Analyst 146 (2021) 3234–3241, 10.1039/D0AN02482A. [PubMed: 33999045]

[7]. Liu T, Choi G, Tang Z, Kshirsagar A, Politza AJ, Guan W, Fingerpick blood-based nucleic acid testing on A USB interfaced device towards HIV self-testing, Biosens. Bioelectron 209 (2022) 114255, 10.1016/j.bios.2022.114255.

[8]. Mauk M, Song J, Bau HH, Gross R, Bushman FD, Collman RG, et al. , Miniaturized devices for point of care molecular detection of HIV, Lab Chip 17 (2017) 382–394, 10.1039/C6LC01239F. [PubMed: 28092381]

[9]. Phillips EA, Moehling TJ, Ejendal KFK, Hoilett OS, Byers KM, Basing LA, et al. , Microfluidic rapid and autonomous analytical device (microRAAD) to detect HIV from whole blood samples, Lab Chip 19 (2019) 3375–3386, 10.1039/C9LC00506D. [PubMed: 31539001]

[10]. Trick AY, Ngo HT, Nambiar AH, Morakis MM, Chen FE, Chen L, et al. , Filtration-assisted magnetofluidic cartridge platform for HIV RNA detection from blood, Lab Chip 22 (2022) 945–953, 10.1039/D1LC00820J. [PubMed: 35088790]

[11]. Wang J, Kreutz JE, Thompson AM, Qin Y, Sheen AM, Wang J, et al. , SD-chip enabled quantitative detection of HIV RNA using digital nucleic acid sequence-based amplification (dNASBA), Lab Chip 18 (2018) 3501–3506, 10.1039/C8LC00956B. [PubMed: 30351338]

[12]. Athamanolap P, Hsieh K, O'Keefe CM, Zhang Y, Yang S, Wang TH, Nanoarray digital polymerase chain reaction with high-resolution melt for enabling broad bacteria identification and Pheno–molecular antimicrobial susceptibility test, Anal. Chem 91 (2019) 12784–12792, 10.1021/acs.analchem.9b02344. [PubMed: 31525952]

[13]. Rane TD, Chen L, Zec HC, Wang TH, Microfluidic continuous flow digital loop-mediated isothermal amplification (LAMP), Lab Chip 15 (2015) 776–782, 10.1039/C4LC01158A. [PubMed: 25431886]

[14]. Rodriguez-Manzano J, Karymov MA, Begolo S, Selck DA, Zhukov DV, Jue E, et al. , Reading out single-molecule digital RNA and DNA isothermal amplification in nanoliter volumes with unmodified camera phones, ACS Nano 10 (2016) 3102–3113, 10.1021/acsnano.5b07338. [PubMed: 26900709]

[15]. Xiang X, Shang Y, Zhang J, Ding Y, Wu Q, Advances in improvement strategies of digital nucleic acid amplification for pathogen detection, TrAC Trends in Analytical Chemistry 149 (2022) 116568, 10.1016/j.trac.2022.116568.

[16]. Xu L, Qu H, Alonso DG, Yu Z, Yu Y, Shi Y, et al. , Portable integrated digital PCR system for the point-of-care quantification of BK virus from urine samples, Biosens. Bioelectron 175 (2021) 112908, 10.1016/j.bios.2020.112908.

[17]. Yin H, Wu Z, Shi N, Qi Y, Jian X, Zhou L, et al. , Ultrafast multiplexed detection of SARS-CoV-2 RNA using a rapid droplet digital PCR system, Biosens. Bioelectron 188 (2021) 113282, 10.1016/j.bios.2021.113282.

[18]. Shen F, Sun B, Kreutz JE, Davydova EK, Du W, Reddy PL, et al. , Multiplexed quantification of nucleic acids with large dynamic range using multivolume Digital RT-PCR on a rotational SlipChip tested with HIV and hepatitis C Viral load, J. Am. Chem. Soc 133 (2011) 17705–17712, 10.1021/ja2060116. [PubMed: 21995644]

[19]. Sun B, Shen F, McCalla SE, Kreutz JE, Karymov MA, Ismagilov RF, Mechanistic evaluation of the pros and cons of digital RT-LAMP for HIV-1 viral load quantification on a microfluidic device and improved efficiency via a two-step digital protocol, Anal. Chem 85 (2013) 1540–1546, 10.1021/ac3037206. [PubMed: 23324061]

[20]. Ding X, Yin K, Li Z, Sfeir MM, Liu C, Sensitive quantitative detection of SARS-CoV-2 in clinical samples using digital warm-start CRISPR assay, Biosens. Bioelectron 184 (2021) 113218, 10.1016/j.bios.2021.113218.

[21]. Luo X, Xue Y, Ju E, Tao Y, Li M, Zhou L, et al. , Digital CRISPR/Cas12b-based platform enabled absolute quantification of viral RNA, Anal. Chim. Acta 1192 (2022) 339336, 10.1016/j.aca.2021.339336.

[22]. Park JS, Hsieh K, Chen L, Kaushik A, Trick AY, Wang TH, Digital CRISPR/Cas-assisted assay for rapid and sensitive detection of SARS-CoV-2, Adv. Sci 8 (2021) 2003564, 10.1002/advs.202003564.

[23]. Politza AJ, Nouri R, Guan W, Digital CRISPR systems for the next generation of nucleic acid quantification, TrAC Trends Analyt. Chem 159 (2023) 116917, 10.1016/j.trac.2023.116917.

[24]. Wu X, Tay JK, Goh CK, Chan C, Lee YH, Springs SL, et al. , Digital CRISPR-based method for the rapid detection and absolute quantification of nucleic acids, Biomaterials 274 (2021) 120876, 10.1016/j.biomaterials.2021.120876.

[25]. Gou T, Hu J, Wu W, Ding X, Zhou S, Fang W, et al. , Smartphone-based mobile digital PCR device for DNA quantitative analysis with high accuracy, Biosens. Bioelectron 120 (2018) 144–152, 10.1016/j.bios.2018.08.030. [PubMed: 30173010]

[26]. Hu F, Li J, Zhang Z, Li M, Zhao S, Li Z, et al. , Smartphone-based droplet digital LAMP device with rapid nucleic acid isolation for highly sensitive point-of-care detection, Anal. Chem 92 (2020) 2258–2265, 10.1021/acs.analchem.9b04967. [PubMed: 31841633]

[27]. Liu X, Wang X, Zhang H, Yan Z, Gaňová M, Lednický T, et al. , Smartphone integrated handheld (SPEED) digital polymerase chain reaction device, Biosens. Bioelectron 232 (2023) 115319, 10.1016/j.bios.2023.115319.

[28]. Ding X, Yin K, Li Z, Liu C, All-in-One Dual CRISPR-Cas12a (AIOD-CRISPR) Assay: a case for rapid, ultrasensitive and visual detection of novel coronavirus SARS-CoV-2 and HIV virus, bioRxiv, (2020) 2020.03.19.998724. 10.1101/2020.03.19.998724.

[29]. Li Z, Uno N, Ding X, Avery L, Banach D, Liu C, Bioinspired CRISPR-mediated cascade reaction biosensor for molecular detection of HIV using a glucose meter, ACS Nano 17 (2023) 3966–3975, 10.1021/acsnano.2c12754. [PubMed: 36762838]

[30]. Chen FE, Lee PW, Trick AY, Park JS, Chen L, Shah K, et al. , Point-of-care CRISPR-Cas-assisted SARS-CoV-2 detection in an automated and portable droplet magnetofluidic device, Biosens. Bioelectron 190 (2021) 113390, 10.1016/j.bios.2021.113390.

[31]. Sun Z, Lin KF, Zhao ZH, Wang Y, Hong XX, Guo JG, et al. , An automated nucleic acid detection platform using digital microfluidics with an optimized Cas12a system, Sci. Chin. Chem 65 (2022) 630–640, 10.1007/s11426-021-1169-1.

[32]. Ngo HL, Nguyen HD, Tran VN, Ngo HT, Development of a low-cost and portable real-time PCR machine for developing countries, in: 8th International Conference on the Development of Biomedical Engineering in Vietnam, Cham, Vietnam, 2022, pp. 69–83.

[33]. Tang R, Yang H, Gong Y, You M, Liu Z, Choi JR, et al. , A fully disposable and integrated paper-based device for nucleic acid extraction, amplification and detection, Lab Chip 17 (2017) 1270–1279, 10.1039/C6LC01586G. [PubMed: 28271104]

[34]. Wan L, Chen T, Gao J, Dong C, Wong AHH, Jia Y, et al. , A digital microfluidic system for loop-mediated isothermal amplification and sequence specific pathogen detection, Sci. Rep 7 (2017) 14586, 10.1038/s41598-017-14698-x. [PubMed: 29109452]

[35]. Wang X, Zhang L, Chen G, Hot embossing and thermal bonding of poly(methyl methacrylate) microfluidic chips using positive temperature coefficient ceramic heater, Anal. Bioanal. Chem 401 (2011) 2657–2665, 10.1007/s00216-011-5377-5. [PubMed: 21922306]

[36]. Redmon J, Divvala S, Girshick R, Farhadi A, You only look once: unified, real-time object detection, in: 2016 IEEE Conference on Computer Vision and Pattern Recognition (CVPR), Las Vegas, NV, USA, 2016, pp. 779–788, 10.1109/CVPR.2016.91.

[37]. Bochkovskiy A, Wang CY, Liao HYM, YOLOv4: optimal speed and accuracy of object detection, arXiv:2004.10934, (2020). 10.48550/arXiv.2004.10934.

[38]. Gardner K, Uddin M, Tran L, Pham T, Vanapalli S, Li W, Deep learning detector for high precision monitoring of cell encapsulation statistics in microfluidic droplets, Lab Chip 22 (2022) 4067–4080, 10.1039/D2LC00462C. [PubMed: 36214344]

[39]. Yao Y, Zhao S, Liang Y, Hu F, Peng N, A one-stage deep learning based method for automatic analysis of droplet-based digital PCR images, Analyst 148 (2023) 3065–3073, 10.1039/D3AN00615H. [PubMed: 37305953]

[40]. Ünel FÖ, Özkalayci BO, Çiğla C, The power of tiling for small object detection, in: 2019 IEEE/CVF Conference on computer vision and pattern recognition workshops (CVPRW), Long Beach, CA, USA, 2019, pp. 582–591.

[41]. Sokolova M, Lapalme G, A systematic analysis of performance measures for classification tasks, Inf. Process Manag 45 (2009) 427–437, 10.1016/j.ipm.2009.03.002.

[42]. Tharwat A, Classification assessment methods, Appl. Comput. Informat 17 (2021) 168–192, 10.1016/j.aci.2018.08.003.

[43]. Yin J, Zou Z, Hu Z, Zhang S, Zhang F, Wang B, et al. , A “sample-in-multiplex-digital-answer-out” chip for fast detection of pathogens, Lab Chip 20 (2020) 979–986, 10.1039/C9LC01143A. [PubMed: 32003380]

[44]. Chen Y, Zheng B, Zhang Z, Wang Q, Shen C, Zhang Q, Deep learning on mobile and embedded devices: state-of-the-art, challenges, and future directions, ACM Comput. Surv 53 (2020) 84, 10.1145/3398209. Article.

[45]. Cai H, Lin J, Lin Y, Liu Z, Tang H, Wang H, et al. , Enable Deep Learning on Mobile Devices: methods, Systems, and Applications, ACM Trans. Des. Autom. Electron. Syst 27 (2022) 20, 10.1145/3486618. Article.

[46]. Breshears LE, Nguyen BT, Akarapipad P, Sosnowski K, Kaarj K, Quirk G, et al. , Sensitive, smartphone-based SARS-CoV-2 detection from clinical saline gargle samples, PNAS Nexus 1 (2022) pgac028, 10.1093/pnasnexus/pgac028.

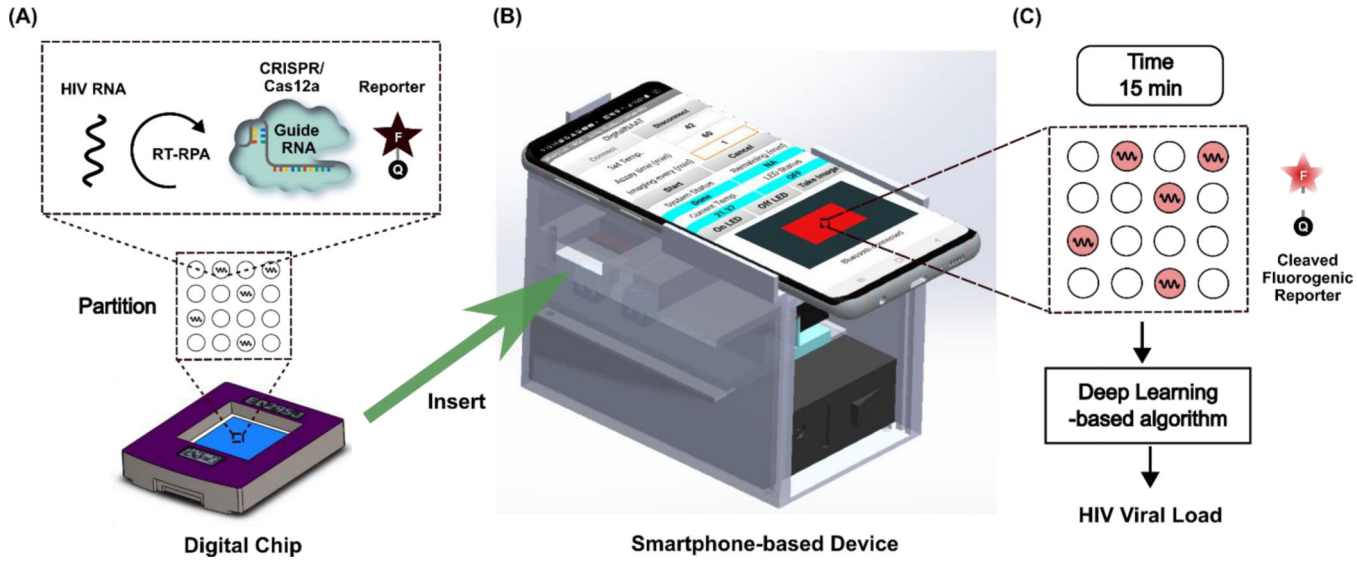

Fig. 1. Overview of smartphone-enabled digital CRISPR device for rapid and portable quantification of HIV viral load.

(A) HIV RNA sample and RT-RPA-CRISPR assay reagents are loaded into a commercial onto QuantStudio digital chip. (B) The digital chip is inserted into the smartphone-based portable device for HIV RNA target amplification and fluorescence imaging using the smartphone camera. (C) After 15 min, the fluorescence image is analyzed by a Deep Learning-based algorithm for HIV viral load estimation.

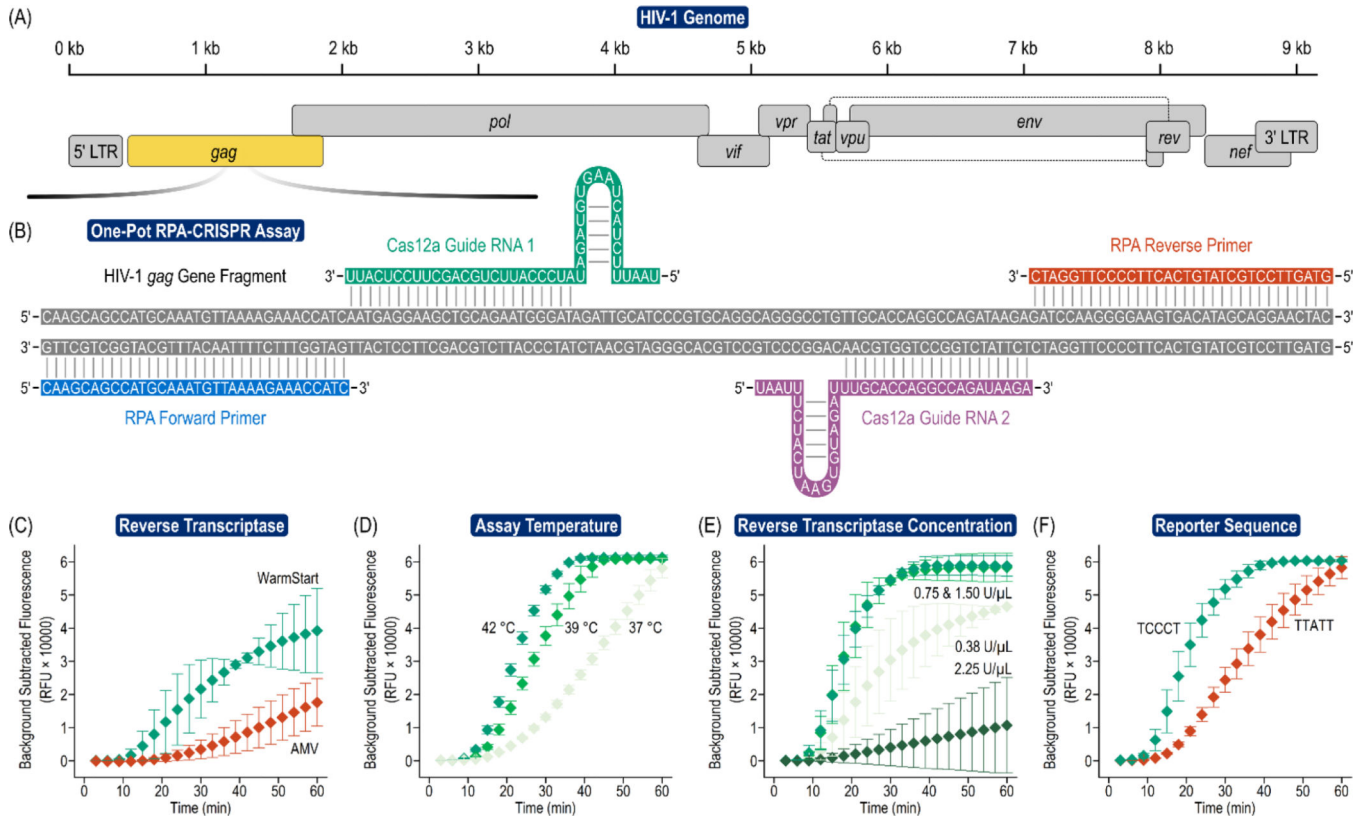

Fig. 2. RT-RPA-CRISPR assay for efficient HIV RNA detection.

(A) The assay is designed to target the HIV-1 *gag* gene by using (B) a pair of RPA primers and a pair of CRISPR/Cas12a guide RNAs that can amplify and detect the target in a single-step within one pot. By tuning (C) the reverse transcriptase, (D) the assay temperature, (E) the reverse transcriptase concentration, and (F) the fluorogenic reporter sequence, the assay can detect 1000 copies HIV RNA – comparable to the effective concentration of a single copy of RNA within the digital reaction well – with plateauing fluorescence signals within 30 min.

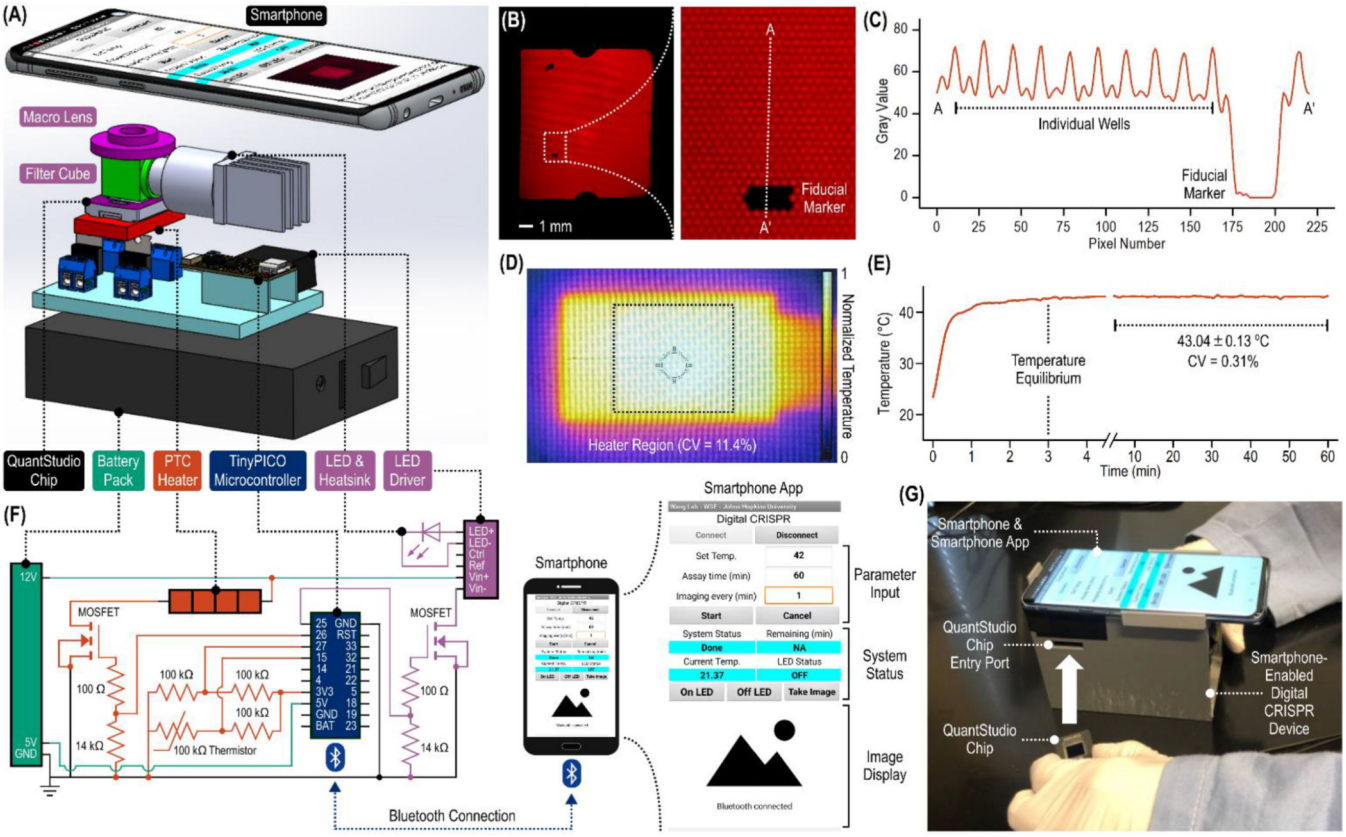

Fig. 3. Palm-size smartphone-enabled digital device.

(A) The key components of the device, besides the smartphone, include a macro lens, a LED (and its accompanying heat sink), a custom fluorescence filter cube, a LED driver, a positive temperature coefficient (PTC) ceramic heater, control circuitry featuring a TinyPICO microcontroller, and a battery pack. The macro lens, the custom fluorescence cube, and the LED (i.e., the fluorescence macrophotography module) endow the smartphone a large field of view for (B) imaging the entire QuantStudio digital chip and sufficient resolution for (C) resolving individual digital wells filled with a fluorescent dye. (D) The compact PTC ceramic heater delivers uniform temperature across the heater region (black dashed box) that is comparable to the size of the QuantStudio chip. (E) Once initiated, the PTC ceramic heater can reach the set temperature in ~3 min and maintain a stable temperature throughout the course of the reaction. (F) The control circuitry includes a TinyPICO microcontroller, a circuit for measuring and controlling the temperature of the PTC ceramic heater, and a circuit for turning the LED on and off. The TinyPICO microcontroller communicates with the smartphone via Bluetooth. A custom smartphone app is developed to input necessary parameters, display system status, and show fluorescence images throughout the assay. (G) All the components of the smartphone-based device are enclosed within a 3D-printed housing, measuring 70 mm × 115 mm × 80 mm ($W \times L \times H$), with a total weight of 575 gs including the smartphone.

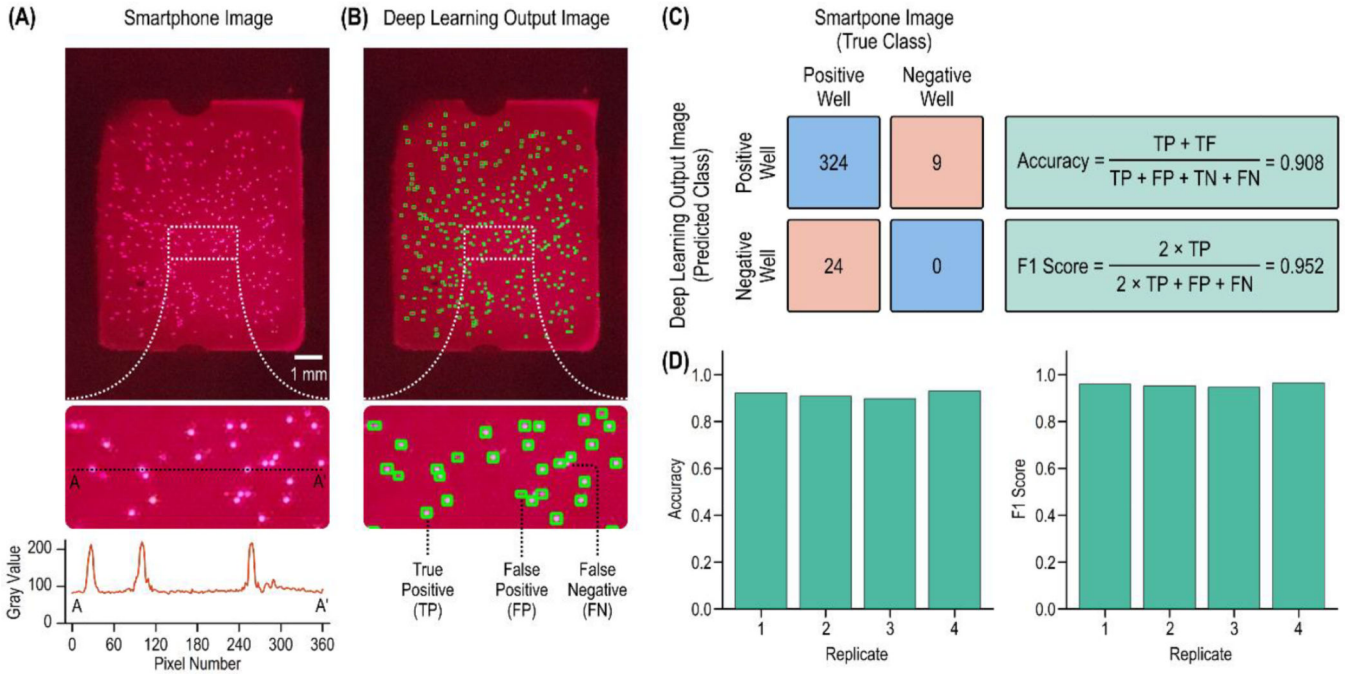

Fig. 4. Deep learning (DL)-based detection of digital RT-RPA-CRISPR.

(A) Successful digital RT-RPA-CRISPR and detection of HIV RNA are indicated by strongly fluorescent digital reaction wells (i.e., positive wells, ~2.5 times higher than the background) observed from the smartphone-acquired image. (B) A DL algorithm is developed to analyze the smartphone image and output an image with detected positive wells, with mostly true positives (i.e., correctly identified positive wells) and some false positives and false negatives (i.e., misidentified wells). (C) When quantitatively compared to the smartphone image as the true class, the DL output image as the predicted class correctly identifies most positive wells, as shown in the confusion matrix, and achieves an accuracy of 0.908 and an F1 score of 0.952. (D) Across 4 technical replicates, the DL algorithm achieves > 0.897 accuracies and > 0.946 F1 scores.

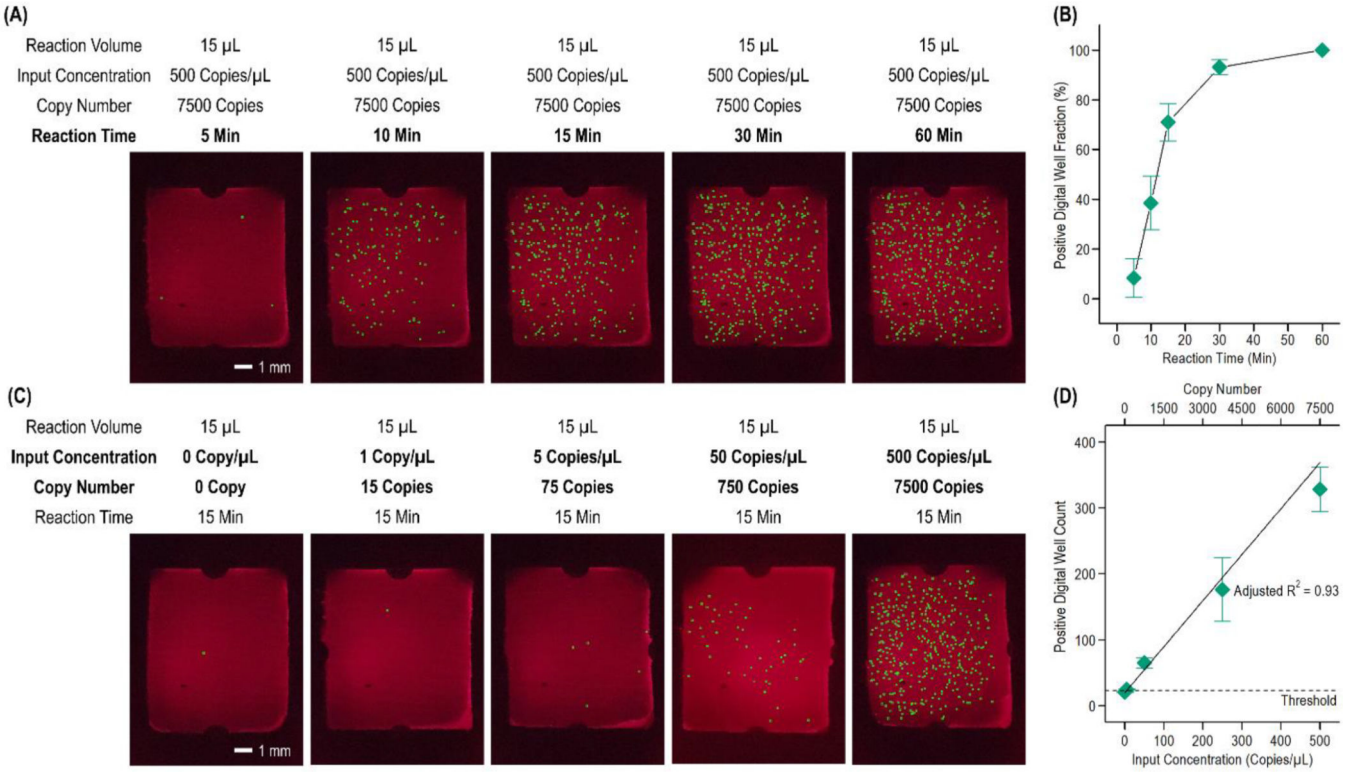

Fig. 5. Rapid and portable quantification of HIV RNA in smartphone-enabled digital CRISPR device.

(A) The device supports real-time monitoring of digital reactions, as illustrated by DL-analyzed QuantStudio chip images of 7500 HIV RNA copies input at 5 min, 15 min, 30 min, and 60 min. (B) Percentage of positive wells detected at these time points normalized to the number of positive wells detected at 60 min reveal that the digital assay can be performed with a shorter assay time such as 15 min and still achieve quantitative detection ($n = 8$; error bars represent standard error of the mean). (C) Upon performing 15 min digital reactions in the smartphone-enabled digital CRISPR device, the resulting DL-analyzed output images of various RNA copy numbers illustrate the capacity for detecting as low as 5 copies/µL, equivalent to 75 copies of HIV RNA in the 15 µL reaction volume within the QuantStudio chip. (D) Replicated results ($n \geq 3$; error bars represent standard error of the mean) at 15 min reaction time using the device and subsequent linear regression analysis confirm the linear relationship between input HIV RNA and number of positive wells. The limit of detection is 75 copies based on the mean + 3SD threshold calculated from the no RNA negative controls.